Size effect anomalies in the behaviour of loaded 3D mechanical metamaterials

Martin Dunn & Marcus Wheel

Department of Mechanical & Aerospace Engineering
University of Strathclyde
Glasgow, G1 1XJ, UK

Abstract

Size effects exhibited by mechanical metamaterials when loaded may be positive such that reducing overall size towards that of the length scale of the underlying structure intrinsic to the material is accompanied by increasing stiffness or rigidity, a phenomenon that has been repeatedly observed and is also forecast by various more generalized continuum theories of deformation in loaded heterogeneous continua. However, such effects may in certain circumstances be contradictory in that decreasing size is accompanied by increasing compliance, the transition from the conventional, positive to this theoretically unanticipated negative behaviour having been explained recently in terms of the distribution of material within 2D continua subject to bending. Here we report on a novel phenomenon newly observed in periodic 3D lattice materials comprised of repeated cubic unit cells formed of exterior edge and interior diagonal connectors. Subtle redistribution of matrix material from edges to diagonals causes the size effect to change dramatically, inverting from positive to negative when loaded in the torsional mode while the corresponding effect for the flexural mode remains entirely positive under the same circumstances. This observation may lead to the prospect of optimising the design of 3D periodic metamaterials to provide a stiffer response in one loading mode and a more compliant response in another, a feature that could potentially be exploited in various innovative applications.

Keywords

Mechanical metamaterial, size effect, Cosserat (micropolar) elasticity, additive manufacturing, 3D printing

1. Introduction

Mechanical metamaterials may exhibit size effects when loaded due to the influence of their internal structure on global deformation. These size effects are characterised by deformations that do not scale conventionally with overall size and thus contradict classical Cauchy elasticity theory which has to date provided the most universally accepted description of the deformation of homogeneous materials. More generalized continuum theories such as couple stress [1,2], micropolar [3,4] (or Cosserat [5]), micromorphic [4] and gradient elasticity [6,7] do account for size effects and incorporate an intrinsic length scale, purportedly reflecting the size of the underlying structure, as an additional constitutive parameter that must be identified empirically. Ordinarily, these more involved theories forecast a positive size effect in which material stiffness increases as the overall size reduces to that associated with the internal structure, behaviour that has indeed been observed in a variety of heterogeneous materials [8,9,10,11,12,13,14,15,16]. Nevertheless, contradictory behaviour in which compliance increases with decreasing size, a contrasting negative effect, has been observed in other materials, notably hard biological tissues [17,18]. Very recently, both conventionally anticipated [19] and more involved [20] size effects have been reported in additively manufactured mechanical metamaterials. Some of these contrasting and more involved effects have been analytically explained for various materials notably those comprised of more rigid periodic inclusions within a compliant matrix [21], layered composite laminates [22] and those formed of periodic 2D lattices [23, 24].

Theoretical and numerical predictions of size effects in materials formed of planar lattices have been derived previously [25,26,27,28,29,30,31], this being motivated by the desire to understand the mechanical behaviour of crystalline materials at the microstructural level as well as fabricated structural materials such as honeycombs. The lattice connectors or elements are usually assumed to be slender and straight with a uniform cross section throughout, all of the same length and connected at their ends only. Furthermore, each connector is generally assumed to possess extensional stiffness along its major axis and flexural stiffness perpendicular to this axis. These assumptions facilitate the representation of the connectors as beam like finite elements. The behaviour of the lattice material can then be established by considering the response of a unit cell comprised of such elements when subjected to a variety of mechanical loadings using either a minimisation of total potential energy based approach [25] or a matrix displacement method [28]. Both have been shown to be equivalent [27]. Lattice materials comprised of square, equilateral triangular and hexagonal unit cells have all been considered and compared in this manner [30]. In each case the predicted behaviour is found to be consistent with that anticipated by Cosserat type generalized continuum theories of deformation. This has enabled the additional constitutive properties, notably the length scale, to be identified in terms of the prescribed connector dimensions and stiffness parameters as appropriate. However, such predictions have been almost universally restricted to the planar case and, in addition, to lattices with a low matrix volume fraction, a consequence of assuming that the connectors are slender. The motivation for our work was to investigate both low and medium density additively manufactured metamaterials based on a lattice or array of cubic unit cells to identify whether the

consistency with the aforementioned deformation theories was maintained at higher dimensionality and matrix volume fraction. Such materials offer significant potential in lightweight structural applications since they are more isotropic than conventional extruded honeycombs and, unlike stochastic open cell foams, their behaviour is deterministic. Therefore, we initially conducted mechanical tests on 3D printed samples of a given volume fraction assembled from unit cells containing only exterior edge connectors of prescribed dimensions. Subsequently we performed extensive finite element analyses using continuum elements to represent similar materials of various volume fractions in which additional interior diagonal connectors were initially absent then subsequently present.

2. Experimental Methods and Numerical Simulations

2.1 Sample Manufacture and Mechanical Testing

Lattice material samples (Figure 1) were printed using a Stratasys OBJET500 Connex3 3D printing machine. The capacity of the printer enables a maximum build size of 342 × 342 × 200mm and thus a unit cell size of 5 × 5 × 5mm with an edge connector half breadth of 1mm was deliberately selected to facilitate manufacture of the largest size samples which comprised of four cells by four cells across their section. The overall length of these samples enabled three point bend testing to be conducted at a maximum length to depth aspect ratio of 16:1. The axial dimension of all sizes of sample was extended by four unit cells so that the samples could be supported inboard of their ends when testing at the prescribed aspect ratio. Sample sets in which the major axis was orientated in the horizontal plane both parallel and perpendicular to the predominant printer head motion were manufactured to ascertain any influence of print direction on flexural stiffness. Samples with their major axis aligned in the vertical direction were not manufactured since the limited machine capacity did not allow this. All samples were printed using the printable photopolymer VeroBlack Plus (RGD875). This is a relatively rigid acrylic based polymer with the manufacturer quoting values of between 2000 and 3000 MPa and from 2200 to 3200 MPa for the Young's and flexural moduli respectively. Overhanging sections of the lattice were supported during printing by a soluble rubber like material that was thoroughly washed away from the polymer matrix prior to testing. The torsion test samples utilised the same unit cell dimensions as the flexural test samples. Again, these samples all had a square cross section, the dimension of which was limited to between two and six unit cells (Figure 2) by the printer capacity which, along with the testing machine capacity, also dictated that all samples now be of the same fixed length, 170 mm, rather than geometrically similar (Figure 2).

Flexural testing of the samples was performed in a Bose Electroforce 3200 mechanical testing machine equipped with a 450N load cell (Figure 3). All samples were loaded at a central deflection rate of 0.08mms^{-1} while being supported within the machine at the prescribed aspect ratio. This deflection rate was applied to each sample for 10s after which the maximum deflection (0.8mm) was maintained for a period of 30s before unloading at the same rate. The force applied to each sample centre was monitored by the load cell throughout the deflection cycle (Figure 4). To identify any influence of manufacturing orientation on the

measured mechanical response each sample was removed from the supports after unloading and rotated by 90° about its major axis before reloading.

Torsion testing was performed using an Instron ElectroPuls E10000 machine incorporating a load cell with a 25Nm torque capacity (Figure 5). To enable rotation transfer from the machine to each sample bespoke couplings comprised of an array of pins that could be precisely inserted into each void located on the sample end sections were custom manufactured. The couplings were deliberately designed to facilitate the distribution of load transfer across the end sections while simultaneously minimizing the suppression of warping of these ends which other attachment methods may not have achieved. However, since each individual pin has a circular cross section this precluded the testing of the smallest viable sample size comprised of a single unit cell across its section. Each sample was twisted at a rate of $0.5°s^{-1}$ for 10s and then held at the maximum rotation (5°) for 30s before unloading at the same rate. The applied torque was measured continuously during the entire loading sequence (Figure 6).

2.2 Finite Element Modelling

Initial finite element models of the manufactured test samples were created by repeatedly regenerating a cubic unit cell in which a structured mesh of 8 noded hexahedral elements (ANSYS element type Solid185) was used to represent the cell edge connectors (Figure 7). A convergence study revealed that four elements through the connector half section were adequate enough to obtain results of sufficient accuracy at reasonable computational cost. The number of element divisions along the connector length was selected to ensure that individual elements retained a cubic shape. Appropriate planes of symmetry were exploited to ensure that overall model size did not become excessive. The Young's modulus and Poisson's ratio for the connector material were specified as 2GPa and 0.3 respectively. The models were constrained in a manner representative of the support conditions imposed in the experiments and a fixed displacement prescribed at the midspan plane of symmetry. Flexural stiffness was determined from the ratio of the resulting reaction force determined at midspan to the prescribed displacement. Subsequent finite element models in which the void volume fraction was varied maintained the same number of elements through connector thickness but the number of divisions along their length was adjusted to preserve the cubic shape of individual elements. The overall length to depth aspect ratio of these models was restricted to 4:1 to maintain a reasonable model size. Consequently, these models were loaded in pure bending rather than three point bending, this being achieved by specifying displacements consistent with a state of prescribed rotation at the end cross sections. Finally, for the finite element models of the lattice material containing diagonal connectors each unit cell was meshed using tetrahedral elements because of the more involved geometry of the intersections between adjoining connectors which precluded the straightforward use of a structured mesh of hexahedral elements.

3. Results and Discussion

3.1 Mechanical Testing Results

The 3D printed samples (Figure 1) of a material comprised of an assembly of cubic unit cells formed of only edge connectors were each loaded in three point bending (Figure 3). While the samples differ in size, ranging from one to four unit cells across their square section, they are nonetheless geometrically similar and therefore have the same length, L, to depth, d, aspect ratio (Figure 1). Although the connectors are printed from an acrylic polymer the samples exhibit an approximately linear relationship between the imposed central displacement and the corresponding measured load (Figure 4). Only slight hysteresis is observed on unloading (Figure 4) so possible viscoelastic effects associated with the polymer matrix have been ignored and hence sample stiffness determined from the gradient of the associated load displacement relationship. Specific flexural stiffness (stiffness per unit sample breadth, b) was found to vary linearly with sample size as measured by the reciprocal of the section dimension squared (Figure 8) with smaller samples exhibiting a greater stiffness than their larger counterparts. In a homogeneous material stiffness would be expected to be size independent due to the geometric scaling. The positive size effect exhibited by the printed material is consistent with Cosserat elasticity theory which predicts the variation in specific flexural stiffness, K/b with size to be [12,15,32]:-

$$\frac{K}{b} = 4E\left(\frac{d}{L}\right)^3\left[1+\frac{1}{24}\left(\frac{l_b}{d}\right)^2\right] \tag{1}$$

for a slender beam when out of plane deformations are neglected. Here E is the flexural modulus and l_b is the characteristic length in bending, an additional material specific constitutive parameter present within the Cosserat theory. The former can be identified from the intercept of the stiffness variation while the latter can be determined from its gradient. The characteristic length in bending, l_b, thus provides a quantitative measure of the observed size effect. For the particular lattice material considered here the values of these parameters ascertained thus ranged from 354 MPa to 430 MPa and from 0.714 mm and 0.986 mm respectively depending on sample print direction and orientation when tested. Matrix anisotropy arising from fabrication thus appears to have some identifiable influence on behaviour. Nevertheless, this is less significant than the influence of size which is evidently associated with the heterogeneous nature of the printed metamaterial.

The material samples of the same length, L, but differing section dimension, d, ranging from two to six unit cells (Figure 2) were tested in torsion (Figure 5). The recorded torque, T, was found to vary linearly with the imposed rotation, θ, and minimal hysteresis was seen on unloading thereby indicating as previously that the material response to loading is predominantly elastic (Figure 6). The torsional stiffness of each sample could thus be identified from the measured response. A solution for the rigidity of a square sectioned prism subjected to twisting [33] when appropriately simplified by assuming that the warping constant, I_P, is the same as that of a prism with a solid square section ($I_P = 2.25d^4/16$) [34],

approximates the variation in torsional rigidity, J ($=TL/\theta$), with cross section dimension, d, as:-

$$J = \frac{TL}{\theta} = G\left[I_P + 2l_t^2 d^2\right] \tag{2}$$

Thus when the normalised torsional rigidity, ($TL/\theta d^2$), is plotted against the sample size as measured by the section dimension squared, d^2, the variation in rigidity when extrapolated does not intersect the origin but exhibits an identifiable positive intercept instead indicating that a size effect is again present (Figure 9). In this case the shear modulus, G, can be determined from the slope of the variation while the characteristic length in torsion, l_t, can be ascertained from the positive intercept. The parameter l_t is analogous to l_b but now provides a quantitative measure of any size effect exhibited in torsion rather than bending. For the 3D lattice material experimentally investigated here G and l_t were thus identified as 38.9 MPa and 1.68mm respectively. Evidently, the shear modulus is an order of magnitude less than the flexural modulus as might be expected given that the lattice is devoid of internal diagonal connectors which if present would significantly enhance torsional stiffness. Nevertheless, the characteristic length in torsion is similar in magnitude to that seen in bending indicating that a distinct positive size effect is again exhibited in this alternative mode of loading.

3.2 Numerical Results

Complementary finite element models of the 3D printed samples were assembled using continuum element representations of each unit cell (Figure 7). Suitable loads and constraints were applied to replicate both loading modes. In the models the polymer matrix was represented by an isotropic linear elastic material with a Young's modulus of 2GPa and a Poisson's ratio of 0.3, the former value having been identified previously from flexural tests on entirely solid samples of the polymer printed with a uniform, continuous cross section. Since matrix isotropy was assumed the influence of sample orientation during manufacture and testing could not be investigated numerically. Nevertheless, all sizes of lattice sample investigated experimentally were also modelled and the variations in both flexural and torsional stiffness with size were thus determined. The flexural modulus and characteristic length in bending identified from the numerically predicted size effect were 351.2 MPa and 0.86 mm respectively. The agreement between these predicted values and their experimentally determined counterparts therefore provides the assurance required in using finite element models exclusively to investigate the mechanical behaviour of additional periodic lattice materials based on a cubic or other suitable unit cell.

After validating the initial finite element predictions against the experimental results additional models of lattice materials based on a cubic unit cell comprised of only edge connectors were then generated. Again, continuum elements were used to represent the connectors but for each sample size the connector cross section dimension was varied so that the effect of matrix volume fraction on stiffness and its variation with size could be established. The additional models were first loaded in pure bending by applying

displacements consistent with constant end rotations, θ, thereby allowing the applied moments, M, to be determined from the computed reactions. By analogy with the torsion case (equation 2), in pure bending the flexural rigidity, D ($=ML/\theta$), is given by:-

$$D = \frac{ML}{\theta} = EI\left[1 + 24\left(\frac{l_b^2}{d^2}\right)\right] \tag{3}$$

where I ($=bd^3/12$) is the second moment of area of the section. Thus, for a square section ($b=d$) when the variation in the normalised flexural rigidity, ($12ML/\theta d^2$), is plotted against sample size, again measured by d^2, and then extrapolated to the vertical axis a size effect will once more be exhibited by a positive intercept from which l_b^2 may otherwise be found. As the cross section of the edge connectors reduces the volume fraction of the void contained within each cell increases as does the characteristic length in bending (Figure 10) implying that the size effect, as measured by l_b^2, not only remains positive but also becomes more apparent with increasing void volume fraction. The additional models were subsequently loaded in torsion. Analogous behaviour was forecast with the characteristic length in torsion increasing as void volume fraction increased (Figure 11) indicating that reducing density is accompanied by a more marked size effect, as quantified by l_t^2, in torsion as well.

Further FE models were generated but with the cubic unit cell now being comprised of both exterior edge and internal diagonal connectors (Figure 12). To reduce the complexity of modelling the geometry of both the intersection between the three diagonal connectors at each cell centre and that of their intersections with the edge connectors at the cell vertices, the cross section of the former was prescribed as circular, with radius R_I, while the cross section of the latter was altered from a square to a quadrant of radius R_E (Figure 13). Thus, when the unit cells were assembled together to form the overall element mesh, all connectors had a circular rather than a square cross section. Consequently, the range of void volume fractions considered was now more limited and varied from around 60% to 98%. This range resulted from specifying three (0.125, 0.25 and 0.5mm) and five (0.125, 0.25, 0.5 0.75 and 1.0mm) different interior and exterior connector radii respectively giving 15 different combinations in total. Due to the more involved geometry tetrahedral rather than hexahedral continuum element were used to mesh the connectors. Again, the models representing samples of different size but each with a square cross section and a constant length were initially loaded in pure bending. For all combinations of connector radii considered a distinct size effect was again observed with the extrapolated flexural rigidity variation with size exhibiting a positive intercept (Figure 14). For each particular combination the characteristic length in bending was derived from the positive intercept identified from the predicted rigidity variation (Figure 14). For each prescribed edge connector radius the size effect, again measured by the characteristic length in bending, increases as the void volume fraction is increased by progressively reducing the interior connector radius (Figure 15) and, furthermore, as the interior connector radius diminishes to zero the characteristic length appears to approach that forecast previously for the samples comprised of unit cells containing edge connectors only suggesting that this provides an upper bound on the possible size effect. Conversely,

increasing internal connector radius evidently suppresses the size effect for a given edge connector radius. Nevertheless, the flexural size effect clearly remains positive for all combinations considered.

When the models of the samples are twisted about their major axis by applying suitable torques an entirely different form of behaviour may be observed depending on the radii prescribed for the internal and external connectors. When the radius of the former is small and that of the latter is large a positive size effect is identifiable from the intercept (figure 16) as in bending. However, as the internal connector radius is increased while the edge connector radius is reduced the size effect, once more quantified by l_t^2, rather than simply being suppressed may completely invert and actually become negative as evidenced by the discernible change in intercept (figure 16) implying that the smaller samples are now more compliant than their larger counterparts. This inversion occurs even when the redistribution of matrix material from edges to diagonals results in almost no change in volume fraction (figure 16). The causes of such size effect inversion have recently been explained for 2D layered [22] and latticed based materials [23,24] loaded in flexure. In the first case a layered material comprised of alternating stiff and compliant layers was shown to exhibit a conventional, positive size effect when the stiffer layers were located furthest from the neutral axis of bending and an opposite, negative effect when the more compliant layers were located thus. In the lattice materials changes to lattice topology that moved the average distribution of material away from the neutral axis resulted in a positive size effect while changes that moved it towards this axis produced a contrasting negative effect. Nevertheless, for the 3D lattice materials investigated here the effect of material distribution is arguably slightly more subtle, increasing internal diagonal connector diameter while simultaneously reducing edge connector diameter redistributes material towards the neutral axes of bending and twisting yet in the former case the size effect is only suppressed as already noted but completely inverts in the latter case. Furthermore, the negative size effect in torsion becomes particularly apparent when the edge connectors are relatively slender and the internal connectors, albeit of of any given diameter, are nevertheless present (figure 17). It should be recognised that for consistency with bending the size effect in torsion has been quantified in terms of l_t^2 using equation 2. For the two specific configurations of similar void volume fraction compared previously (figure 16) it is interesting to note that the value of l_t^2, identified in the case where the edge connectors are more slender ($l_t^2 \approx -0.75$) is comparable in magnitude to that determined when the internal diagonal connectors are more slender ($l_t^2 \approx 1.2$) implying that the associated size effects, while different in nature, are similar in scale. Although the identification of l_t^2 values that are less than zero (figure 17) using equation 2 provides a means of quantifying the size effect when negative it implies that valid, material specific values of l_t cannot then be identified for any of these cases. This apparent invalidity occurs because generalised continuum theories of the Cosserat type customarily forecast a positive size effect (equation 2) so interpreting a negative size effect within the context of such theories indicates that there may be a limitation in their applicability particularly when the unit cell size is comparable to the overall size as has been investigated here. However, it is at these scales that size effects are most significant and forecasting them becomes more

necessary since when the unit cell size is much smaller than the overall size these theories, though possibly more applicable, anticipate that any size effect will be much less evident.

4. Conclusions

As mentioned earlier, the observation of size effects in a heterogeneous medium is not new, although previous reports of such effects have usually indicated that reducing overall size to that of the length scale of the underlying material heterogeneity will be accompanied by an increase in material stiffness or rigidity, behaviour described here as a conventional or positive effect which concurs with that forecast by more generalised deformation theories such as Cosserat (micropolar) elasticity. While more recent research [22,23,24] has indicated that 2D materials may exhibit both conventional positive and contradictory negative size effects when loaded in bending, the results presented here indicate that the nature of these effects may be even more involved than existing theoretical forecasts would imply or any previous work has identified. The complete inversion of the size effect from positive to negative in braced open cell cubic lattices subject to twisting while the corresponding effect in bending remains positive is an entirely new result that cannot be adequately predicted by such theories. In reporting this result we aim to inspire further research and development in three complementary fields. Firstly, the inability of existing more generalised continuum theories to adequately predict it indicates that these theories either require enhancing or need to be superseded by new ones capable of providing a more satisfactory prediction. Clearly, this is an impending imperative for the theoretical continuum mechanics field. Secondly, further empirical investigation of alternative metamaterials such as closed cell foams with a periodic structure is required to determine whether the anomalous size effects reported here are also exhibited by such materials. This is suggested as part of the forthcoming agenda for both the experimental and computational mechanics fields. Finally, and of most practical significance, we seek to stimulate the premeditated design of bespoke metamaterials whose stiffness in different loading modes can be optimised by selecting the appropriate size scale for the periodic internal structure. Interestingly, this might involve maximising stiffness in one mode while minimising it in another. As noted very recently [35], behaviour of this kind has traditionally been regarded as more of a burden than an opportunity in design, yet it has significant potential in many practical application areas such as, for example, sandwich panel structures where it may be possible to optimize the configuration of a core material based on a periodic 3D lattice to simultaneously promote flexural stiffness and torsional compliance. Such structures might then be of real utility in applications such as self pitching aerodynamic control surfaces.

Acknowledgements

The financial support of the Engineering and Physical Sciences Research Council through a Doctoral Training Grant (grant number EP/L505080/1) for Martin Dunn is acknowledged.

Declaration of Interests

No conflicts of interest were reported by the authors

References

1. R.A. Toupin, Elastic materials with couple stresses, Arch. Ration. Mech. Anal., 11, 385-414 (1962)
2. R.D. Mindlin & H.F. Tiersten, Effects of couple-stresses in linear elasticity, Arch. Ration. Mech. Anal., 11, 415-448 (1962)
3. A.C. Eringen, Linear theory of micropolar elasticity. Journal of Mathematics and Mechanics, 15, 909–923 (1966)
4. A.C. Eringen, Microcontinuum Field Theories I: Foundations and Solids. Springer-Verlag New York (1999)
5. E. Cosserat & F. Cosserat, Theorie des Corps Deformables, Hermann, Paris (1909).
6. R.D. Mindlin, Microstructure in linear elasticity, Arch. Rat. Mech. Anal. 16, 51–78 (1964)
7. R.D. Mindlin, Second gradient of strain and surface tension in linear elasticity, Int. J. Solids & Struct.1, 417–438 (1965)
8. J.F.C. Yang and R.S. Lakes, Experimental study of micropolar and couple stress elasticity in bone in bending. Journal of Biomechanics, 15, 91–98 (1982)
9. R.S. Lakes, Size effects and micromechanics of a porous solid. Journal of Materials Science, 18, 2572–2580 (1983)
10. R.S. Lakes, Experimental microelasticity of two porous solids. International Journal of Solids and Structures, 22, 55–63 (1986)
11. W.B. Anderson & R.S. Lakes, Size effects due to Cosserat elasticity and surface damage in closed-cell polymethacrylimide foam. J. Mater. Sci. 29 (24), 6413-6419 (1994)
12. A.J. Beveridge, M.A. Wheel & D.H. Nash, The Micropolar Elastic Behaviour of Model Macroscopically Heterogeneous Materials, International Journal of Solids & Structures, 50, 246-255 (2013)
13. A. Waseem, A.J. Beveridge, M.A. Wheel, & D.H. Nash, The influence of void size on the micropolar constitutive properties of model heterogeneous materials, European Journal of Mechanics A: Solids. 40, 148-157 (2013)
14. M. McGregor & M.A. Wheel, On the coupling number and characteristic length of micropolar media of differing topology, Proceedings of the Royal Society A, 470 (2014)
15. R.S. Lakes & W. Drugan, Bending of a Cosserat elastic bar of square cross section:- theory and experiment, Journal of Applied Mechanics, 82, 1-8 (2015)
16. Z. Rueger & R.S. Lakes, Experimental Cosserat elasticity in open cell foam, Philosophical Magazine, 96, 93-111 (2016)
17. K. Choi, J.L. Kuhn, M.J. Ciarelli & S.A. Goldstein, The elastic moduli of human subchondral, trabecular, and cortical bone tissue and the size-dependency of cortical bone modulus. Journal of Biomechanics, 23(11), 1103-1113 (1990)
18. J.C. Frame, M.A. Wheel & P.E. Riches, A numerical investigation and experimental verification of size effects in loaded bovine cortical bone, International Journal for Numerical Methods in Biomedical Engineering, 34:e2903 (2018)
19. Z. Rueger & R.S. Lakes, R.S., Strong Cosserat elasticity in a transversely isotropic polymer lattice, Physical Review Letters 120 (065501) (2018)

20. C. Coulais, C. Kettenis, & M. van Hecke, A characteristic length scale causes anomalous size effects and boundary programmability in mechanical metamaterials, Nature Physics, 14, 40-44 (2018)
21. D. Bigoni & W.J. Drugan, Analytical derivation of Cosserat moduli via homogenization of heterogeneous elastic materials, Journal of Applied Mechanics, 74, 741-753 (2007)
22. M.A. Wheel, J.C. Frame & P.E. Riches, Is Smaller Always Stiffer? On Size Effects In Supposedly Generalized Continua, International Journal of Solids and Structures (67-68), 84-92 (2015)
23. M. Yoder, L. Thompson, J. Summers, Size effects in lattice structures and a comparison to micropolar elasticity, International Journal of Solids and Structures 143, 245-261 (2018)
24. M. Yoder, L. Thompson, J. Summers, Size effects in lattice-structured cellular materials: edge softening effects, Journal of Materials Science, 54, 3942-3959 (2019)
25. A. Askar & A.S. Cakmak, A structural model of a micropolar continuum, International Journal of Engineering Science, 6, 583-589 (1968)
26. C.B. Banks & M. Sokolowski, On certain two-dimensional applications of the couple stress theory. International Journal of Solids and Structures, 4, 15–29 (1968)
27. Z.P. Bažant & M. Christensen, Analogy between micropolar continuum and grid frameworks under initial stress, International Journal of Solids and Structures, 8, 327-346 (1972)
28. X.L. Wang & W.J. Stronge, Micropolar theory for two-dimensional stresses in elastic honeycomb, Proceedings Royal Society London A, 455, 2091-2116 (1999)
29. A.J. Wang & D.L McDowell, In-plane stiffness and yield strength of periodic metal honeycombs, ASME Journal of Engineering Materials, 126, 137–156 (2004)
30. A. Spadoni & M. Ruzzene, Elasto-static micropolar behaviour of a chiral auxetic lattice, Journal of the Mechanics and Physics of Solids, 60, 156-171 (2012)
31. S. Liu & W. Su, Effective couple-stress continuum model of cellular solids and size effects analysis, International Journal of Solids and Structures, 46, 2787-2799 (2009)
32. F.Y. Huang, B.H. Yan, J.L. Yan & D.U. Yang, Bending analysis of micropolar elastic beam using a 3-D finite element method. International Journal of Engineering Science, 38, 275–286 (2000)
33. H. Park, & R.S. Lakes, Torsion of a micropolar elastic prism of square cross section, International Journal of Solids and Structures, 23, 485-503 (1987)
34. R.J. Roark, W.C. Young, & R. Plunkett, Formulas for stress and strain, McGraw Hill, 7th ed. (2002)
35. M. Kadic, T. Frenzel & M. Wegener, When size matters, Nature Physics, 14, 8-9 (2018)

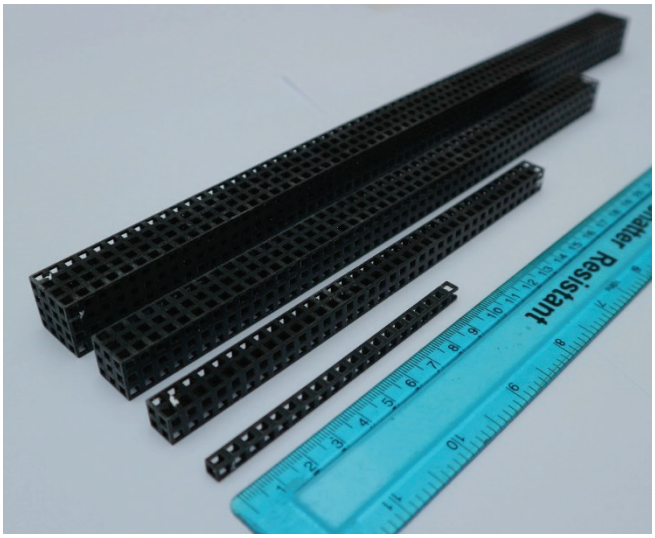

Figure 1: Metamaterial samples of various sizes for flexural testing

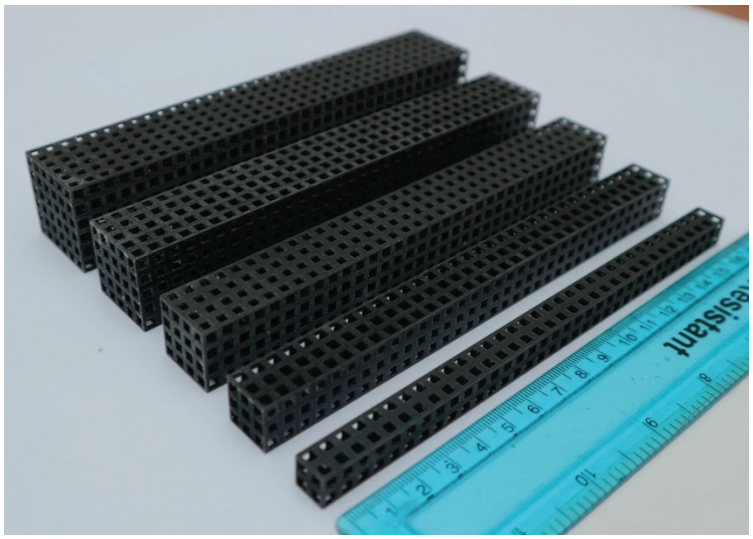

Figure 2: Metamaterial samples of various sizes for torsion testing

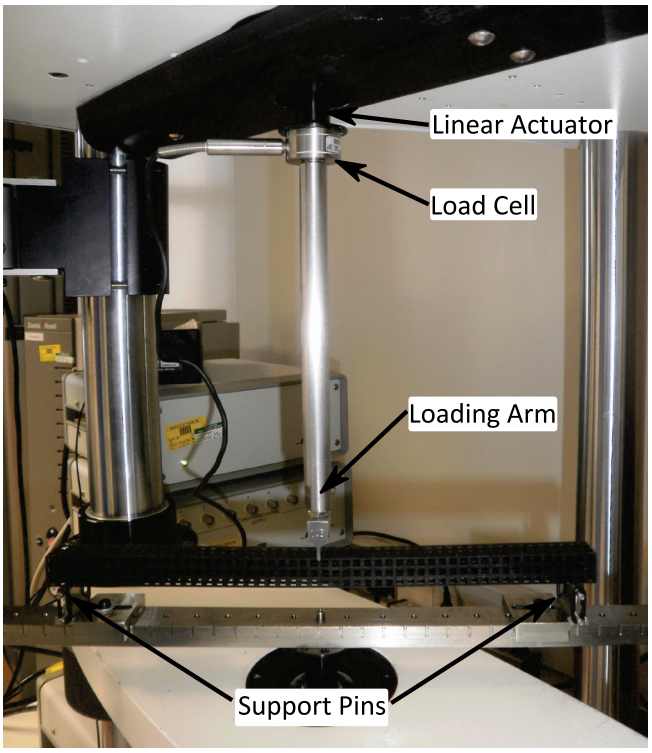

Figure 3: Metamaterial sample being loaded in three point bending

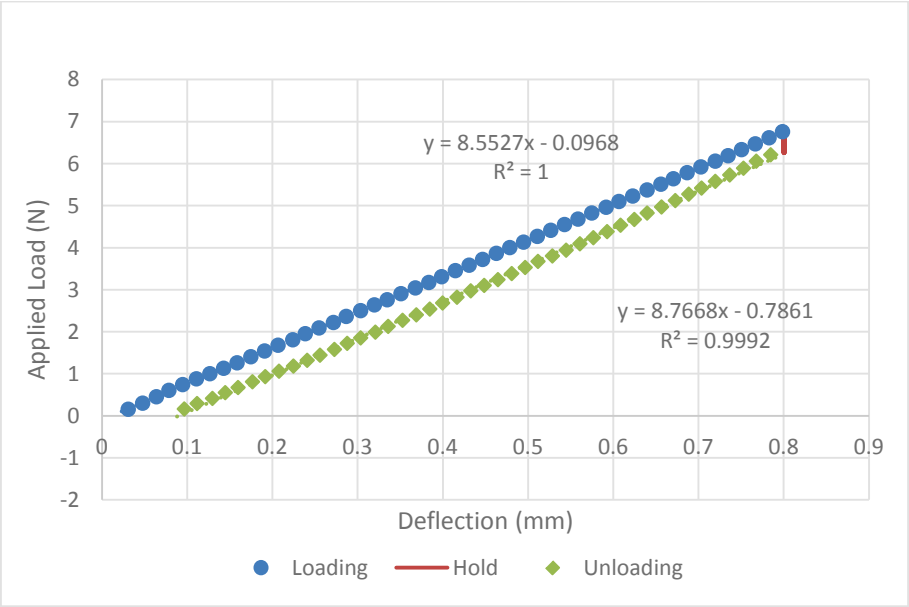

Figure 4: Measured load deflection data for typical sample

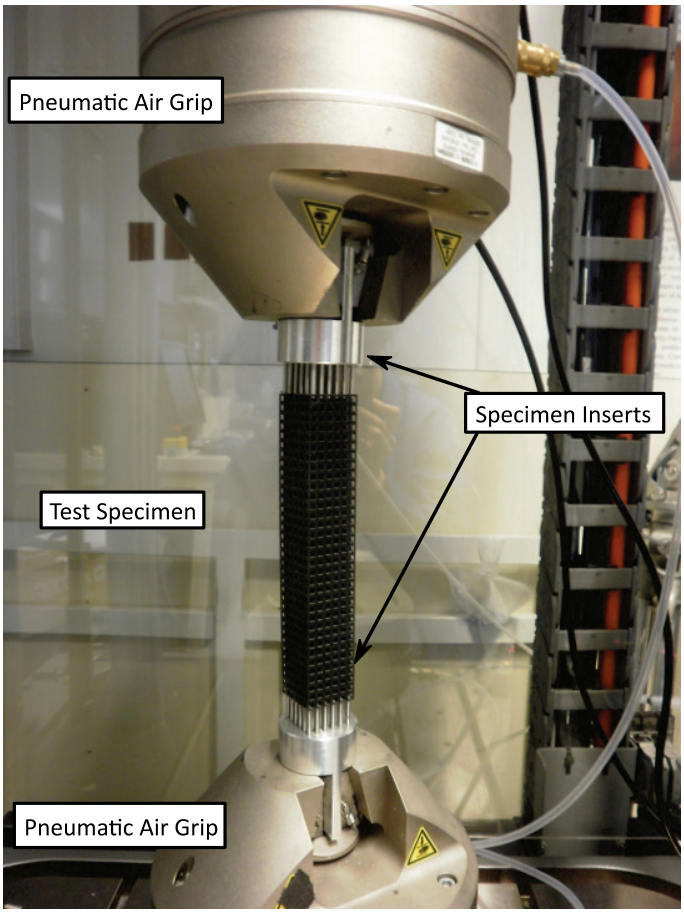

Figure 5: Metamaterial sample being loaded in torsion

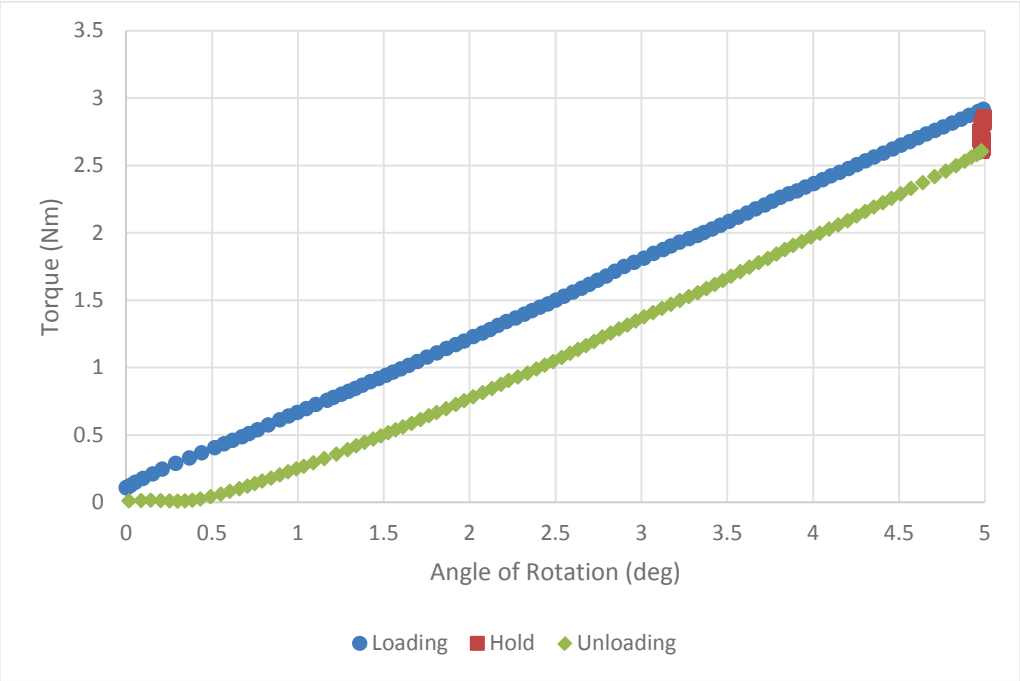

Figure 6: Measured torque rotation data for typical sample

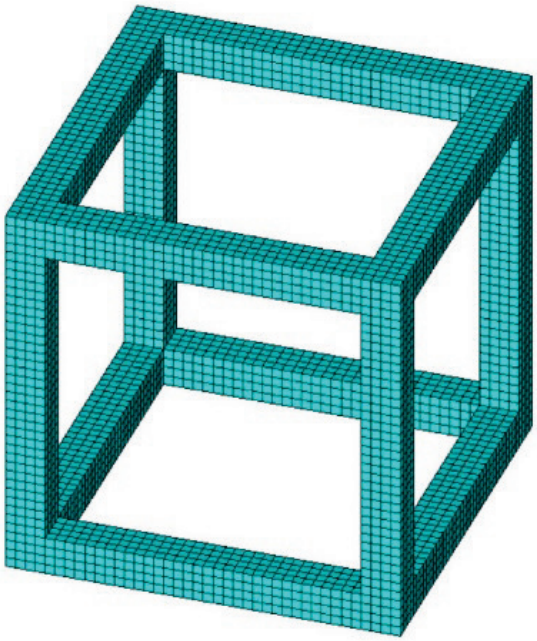

Figure 7: Structured finite element mesh used to represent single unit cell

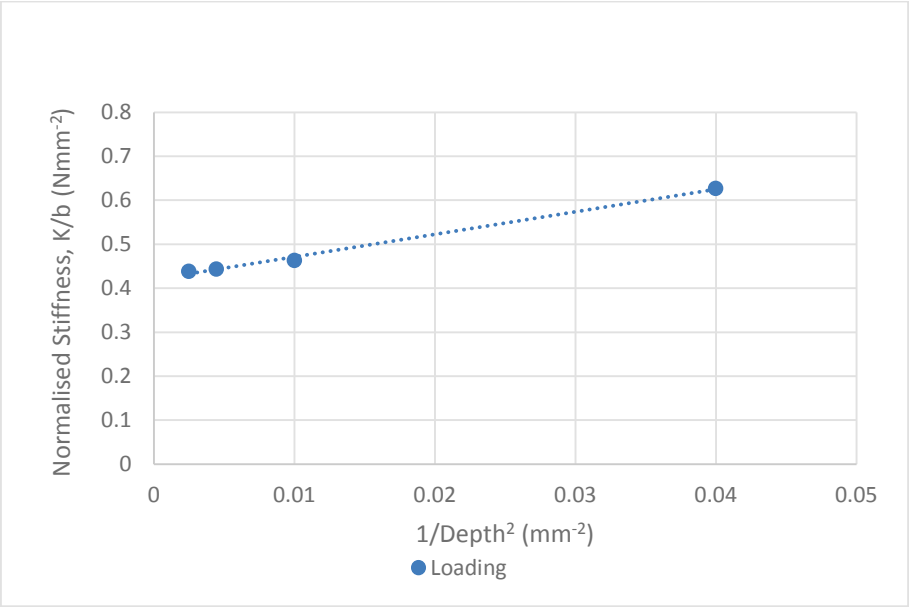

Figure 8: Variation in specific stiffness with sample size as quantified by ($1/d^2$)

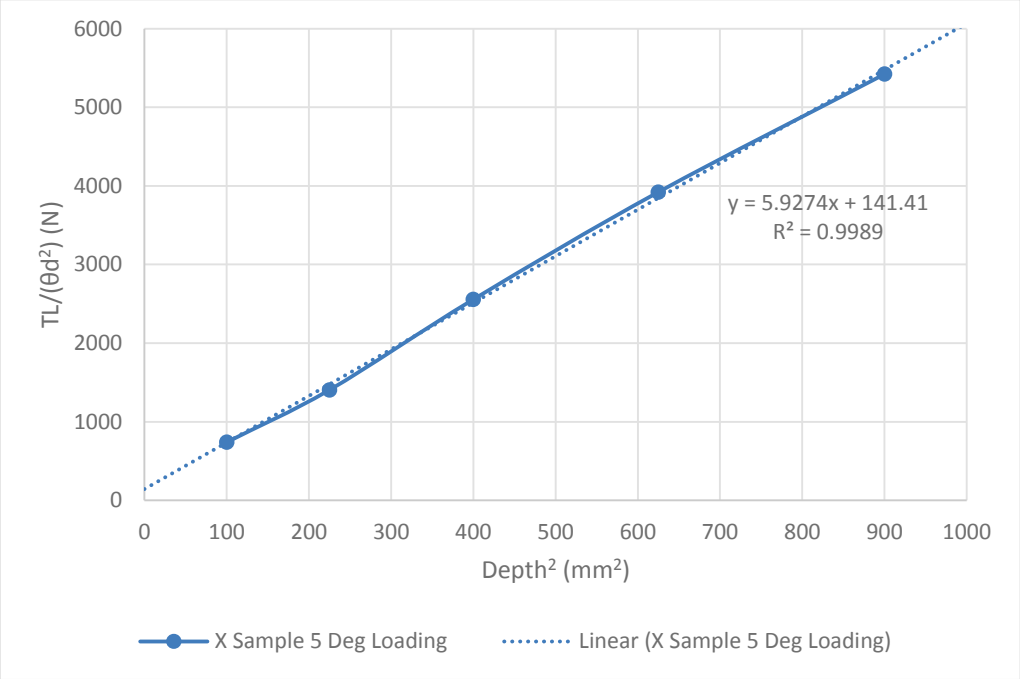

Figure 9: Variation in normalised rigidity with sample size as quantified by d^2

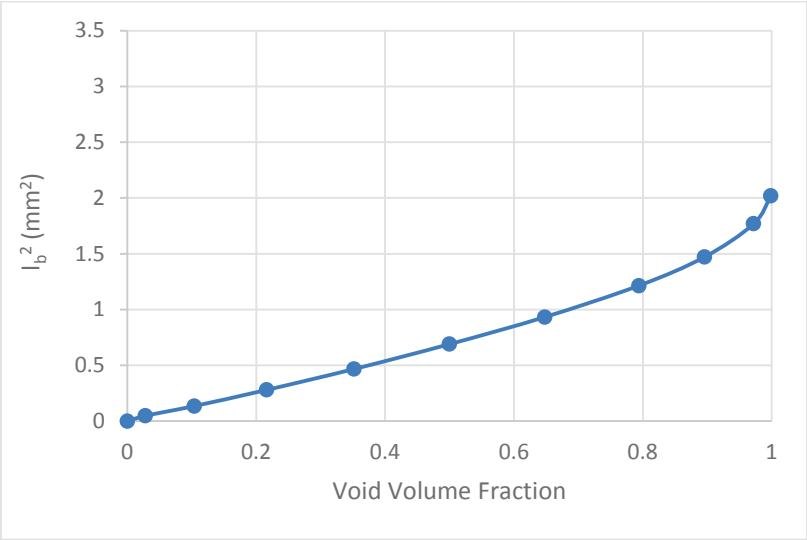

Figure 10: Variation in characteristic length in bending, l_b^2, with void volume fraction

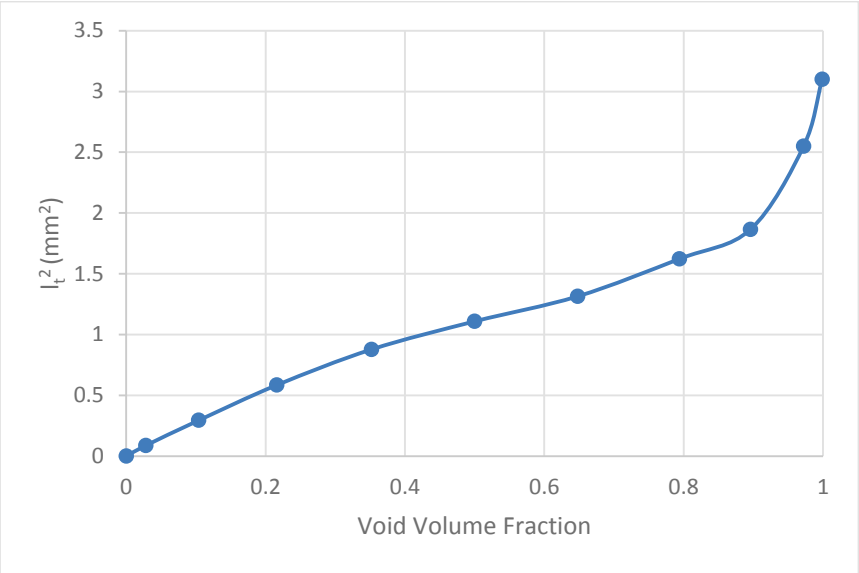

Figure 11: Variation in characteristic length in torsion, l_t^2, with void volume fraction

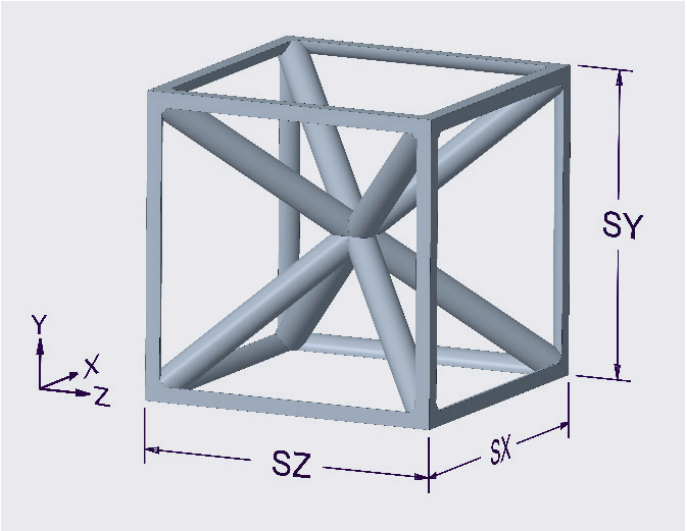

Figure 12: Unit cell with exterior edge and internal diagonal connectors

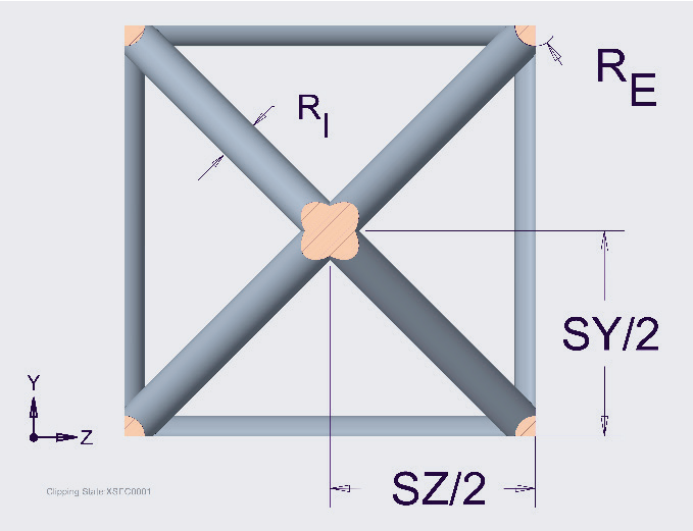

Figure 13: Plane of symmetry of cell through its centre parallel to any face showing connector cross sections

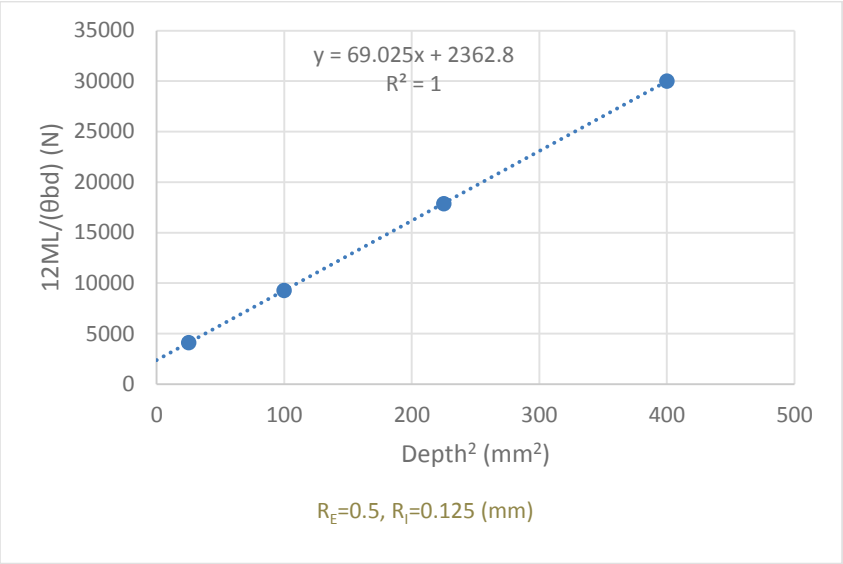

Figure 14: Numerically predicted variation in normalised flexural rigidity with sample size when loaded in pure bending

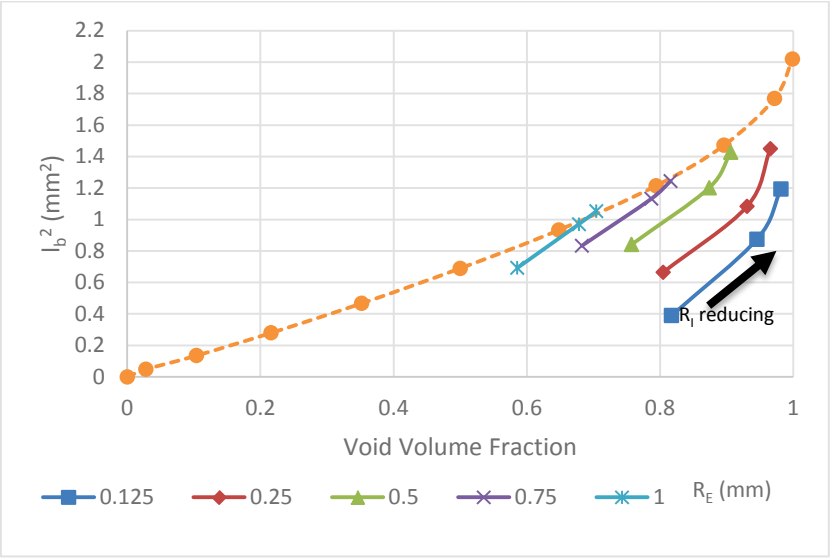

Figure 15: Variation in characteristic length in bending, l_b^2, with void volume fraction for all connector radius combinations (dashed line represents a unit cell with no internal connectors)

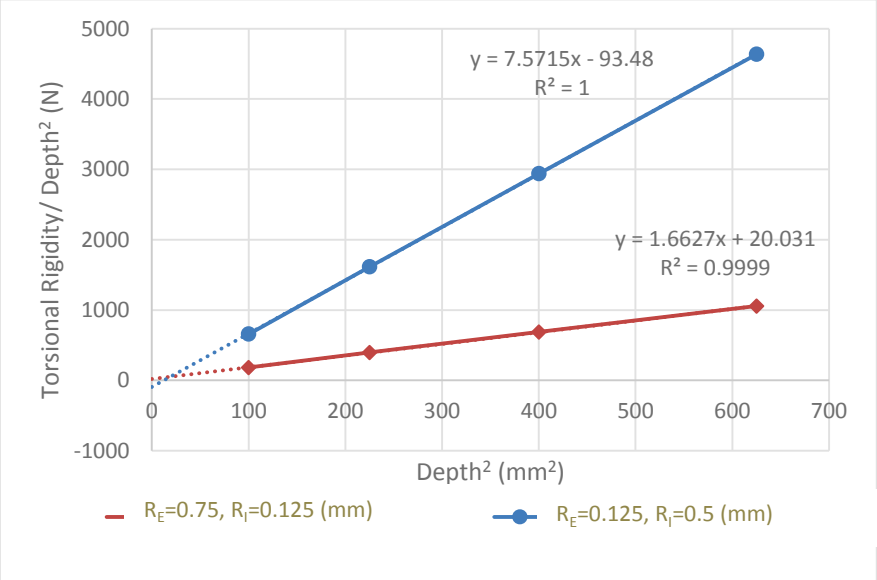

Figure 16: Numerically predicted variation in normalised torsional rigidity with sample size when loaded in torsion for two metamaterials with diagonal connectors and the same volume fraction (≈81.6%) but different connector radii

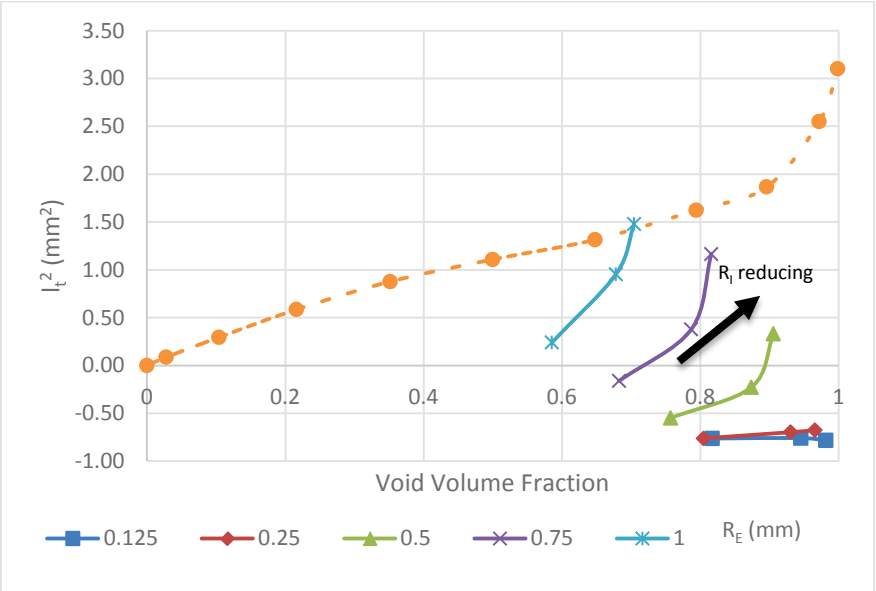

Figure 17: Variation in characteristic length in torsion, l_t^2, with void volume fraction for all connector radius combinations (dashed line represents a unit cell with no internal connectors)

Figure Captions

Figure 1: Metamaterial samples of various sizes for flexural testing

Figure 2: Metamaterial samples of various sizes for torsion testing

Figure 3: Metamaterial sample being loaded in three point bending

Figure 4: Measured load deflection data for typical sample

Figure 5: Metamaterial sample being loaded in torsion

Figure 6: Measured torque rotation data for typical sample

Figure 7: Structured finite element mesh used to represent single unit cell

Figure 8: Variation in specific stiffness with sample size as quantified by $(1/d^2)$

Figure 9: Variation in normalised rigidity with sample size as quantified by d^2

Figure 10: Variation in characteristic length in bending, l_b^2, with void volume fraction

Figure 11: Variation in characteristic length in torsion, l_t^2, with void volume fraction

Figure 12: Unit cell with exterior edge and internal diagonal connectors

Figure 13: Plane of symmetry of cell through its centre parallel to any face showing connector cross sections

Figure 14: Numerically predicted variation in normalised flexural rigidity with sample size when loaded in pure bending

Figure 15: Variation in characteristic length in bending, l_b^2, with void volume fraction for all connector radius combinations (dashed line represents a unit cell with no internal connectors)

Figure 16: Numerically predicted variation in normalised torsional rigidity with sample size when loaded in torsion for two metamaterials with diagonal connectors and the same volume fraction (≈81.6%) but different connector radii

Figure 17: Variation in characteristic length in torsion, l_t^2, with void volume fraction for all connector radius combinations (dashed line represents a unit cell with no internal connectors)